ABSTRACT

Köck, Franz Alexander M. Thermionic Emission from Doped and Nanocrystalline Diamond. (Under the direction of Robert J Nemanich)

Microwave Plasma assisted Chemical Vapor Deposition (MPCVD) has been utilized to synthesize nitrogen doped and intrinsic nanocrystalline diamond films to investigate thermionic field emission behavior. Sulfur-doped nanocrystalline diamond films prepared by hot filament chemical vapor deposition (HFCVD) have been included in the thermionic field emission measurements. The samples were imaged in UHV by photo electron emission microscopy (PEEM) using a UV Hg lamp for photoemission excitation. The same instrument was used to obtain the thermionic-field emission electron microscopy images (T-FEEM) at temperatures up to 900ºC. The Raman spectra of the films showed a strong diamond peak at 1332cm^{-1} and weaker signal from the graphitic regions in the sample. Field emission could not be measured at room temperature, but the PEEM images showed relatively uniform emission. The PEEM images showed little change as the temperature is increased. At temperatures as low as 640ºC the T-FEEM images exhibited strongly enhanced electron emission with increasing temperature. Doped and undoped nanocrystalline diamond films showed localized emission from small emission sites with a significant temperature dependence of the electron emission for the sulfur doped films at around 600ºC. This thesis focuses on developing a consistent model of thermionic emission from doped and nanocrystalline diamond films.

Thermionic Emission from Doped and Nanocrystalline Diamond

Franz Alexander M. Köck
www.franzkoeck.net

A thesis submitted to the Graduate Faculty of
North Carolina State University
in partial fulfillment of the
requirements for the Degree of
Masters of Science

Department of Physics

Raleigh, NC

2003

Approved by

_____
chairman of committee

_____

_____

Παντα ρει

-Heraclitus-

Biography

Franz Alexander M. Köck was born on the 1st December in Vienna, Austria. He started elementary school in a St. Veit / Gölsen, a small village in lower Austria from where he transferred to high school (Bundesrealgymnasium Lilienfeld) in the nearby town of Lilienfeld. After completion he attended military service for the republic of Austria.

His academic education started at the Johannes Kepler Universität in Linz, Austria with a major in physics. The research topic was focused on molecular beam epitaxy of PbTe and PbTe/EuTe and growth characterization by scanning tunneling and atomic force microscopy. With this background he decided to start an exchange semester at North Carolina State University in Raleigh, NC in Dr. Schetzina's laboratory where he did research on the growth of GaN by MBE and characterization by photoluminescence. After finishing he returned to Austria only to come back to North Carolina State University to start graduate school with a physics major. Since then his main research in Dr. Nemanich's laboratory was focused on carbon based materials and their electronic properties, especially electron emission.

Acknowledgements

I would like to acknowledge all members of the SSL group for making this thesis possible.

I gratefully acknowledge support from Frontier Carbon Technology (FCT) under Dr. Koji Kobashi.

Table of Contents

List of Figures

I. Introduction

Diamond exhibits with unique electrical and mechanic properties that avail it to a wide set of applications. Hardness, high thermal conductivity, high carrier mobilities and saturated carrier velocities (high speed), wide bandgap, radiation hardness and chemical inertness promise diamond to be superior than other materials for specific electronic and microelectromechanical system (MEMS) devices [1, 2]. Recently, there has been high interest in the electron emission properties of diamond to be used as an electron source for display applications. These considerations are based on the ability of diamond to exhibit a negative electron affinity (NEA) [3, 4]. An NEA enables electrons from the conduction band minimum to escape the diamond structure without an energy barrier at the surface. One way to achieve NEA characteristics is through hydrogen passivation of the diamond surface. [5] Other processes include deposition of thin metal layers like Ti. To determine whether the surface exhibits a NEA, photoexcitation can be employed to promote electrons into the conduction band minimum and observe if emission occurs. Moreover, Photo Electron Emission Microscopy (PEEM) can be utilized to image the emission properties in a controlled UHV environment. In addition to photoelectron emission, field emission studies can be conducted (FEEM) with the same equipment. [6]

From natural occurring diamond it has been found that the p-type semiconducting property comes from incorporated boron (B) atoms that act as acceptors in the bulk with an energy level of 0.37eV above the top of the valence band. [7] Introducing boron into the diamond lattice gives the crystal a characteristic blue color. The Hope diamond with its deep blue color is the most prominent example of a boron doped natural diamond. The

other dominant impurity in natural diamond is nitrogen (N). Nitrogen is a group V element next to carbon (C) in the periodic table making it the most probable substitutional donor in diamond. [8] The presence of high concentrations of nitrogen can induce a yellow tint of the diamond crystal. It forms a deep donor 1.7eV below the top of the conduction band. Another impurity that is topic of ongoing research is sulfur. The theoretical activation energy of 0.375eV has been observed in experimental temperature dependence plots. [9, 10] Measurements on sulfur doped diamond performed by Sakaguchi *et al.* have furthermore shown a strong increase in the carrier concentration from about $10^{13}cm^{-3}$ at room temperature to about $10^{16}cm^{-3}$ at 300ºC with a maximum in the mobility at room temperature that moderately decreases with the relationship of $T^{-1.5}$. [11]

In this work we have found significant differences in the thermal emission properties of B- doped and N-doped diamond as well as undoped and sulfur doped nanocrystalline diamond. With increasing temperature N-doped diamond films and S-doped nanocrystalline diamond films exhibit strongly enhanced electron emission, whereas B-doped diamond and undoped nanocrystalline diamond show electron emission that remains constant over a wide temperature range.

Thermionic electron emission dates back to pre-semiconductor times when electron tubes were used in electronic circuits. Since then the search for efficient electron sources have become an important part in e.g. display and microwave applications. The basic principle is to thermally excite electrons and remove them from the emitter by applying a sufficient electric field. In the case of a metal emitter the electron has to overcome the work function in order to leave the material. With work function values of

several eV, high temperatures are needed to release electrons into vacuum. For a conventional thermionic emitter the saturated current density is described by the Richardson-Dusham equation

$$J_s = 120T^2 e^{-\frac{e\phi}{k_B T}}$$

where ϕ is the work function of the material.

Thermionic emission from semiconductors usually has to include the electronic structure of the materials in addition to alterations of this structure due to applied electric fields which will be discussed in the following chapters.

To compare the surface morphology of the diamond films with the results from PEEM measurements, atomic force microscopy (AFM) was employed to study topography and to compare it with electron emission sites on the surface. For metallic surfaces, sharp surface features exhibit high field enhancement and thus a high electron emission. From this we may expect that sites that show high electron emission can result from surface features that can be resolved by techniques other than PEEM. Flat surfaces detected by surface investigation tools like AFM would be expected to show no preferred localized electron emission at room temperature. Even with the NEA surface that we find for hydrogen passivated diamond surfaces electron emission would not be observed at room temperature if there are no electrons in the conduction band that could contribute to an emission current. In this thesis I discuss phenomena to promote electrons from levels below the conduction band into the conduction band which can then be released into vacuum because of the NEA characteristic of the hydrogen terminated surface.

This thesis is a comprehensive discussion of three papers published in *Diamond and Related Materials*:

Imaging electron emission from diamond film surfaces: N-doped diamond vs. nanostructured diamond

Diamond and Related Materials, Volume 10, Issues 9-10, September-October 2001, Pages 1714-1718

F. A. M. Köck, J. M. Garguilo and R. J. Nemanich

Enhanced low-temperature thermionic field emission from surface-treated N-doped diamond films

Diamond and Related Materials, Volume 11, Issues 3-6, March-June 2002, Pages 774-779

F. A. M. Köck, J. M. Garguilo, Billyde Brown and R. J. Nemanich

Spatial distribution of electron emission sites for sulfur doped and intrinsic nanocrystalline diamond films,

*Diamond and Related Materials, **In Press, Corrected Proof**, Available online 19 March 2003,*

F. A. M. Köck, J. M. Garguilo, R. J. Nemanich, S. Gupta, B. R. Weiner and G. Morell

II. Experimental Details:

N-doped diamond and undoped nanocrystalline diamond films were grown on 25mm diameter Si <100> substrates with low resistivity of 1Ω·cm and on mirror polished molybdenum squares of 9x9mm. Si sample preparation started with ultrasonic abrasion in a titanium-diamond-ethanol suspension for 30 minutes and a rinse in ethanol for 1 minute. The substrate was then dried with nitrogen gas. Mo samples were mirror polished with diamond paste and after ultrasonically cleaning in acetone and methanol each for 10 minutes the Mo square was dried with nitrogen and afterwards ultrasonically treated with the titanium-diamond-ethanol suspension for 30 minutes. The samples were then rinsed with Ethanol. After loading the sample into the CVD reactor, the chamber was evacuated with a mechanical pump for 60 minutes and the substrate was heated to 150ºC.

The ASTeX IPX3750 microwave assisted CVD system allows a microwave power up to 1500W at a frequency of 2.45GHz. For substrate heating a RF induction heated graphite susceptor is employed with a temperature range up to 1200ºC. The temperature was also monitored with an optical pyrometer.

Process gases, of zero grade N_2, H_2 and CH_4 were used to deposit the films. The CVD reactor was vented with Ar gas when loading a substrate. The flows of the process gases were monitored and controlled with mass flow controllers (MFC).

During film growth laser reflectance interferometry (LRI) was employed for in situ monitoring of the diamond layer thickness.

The growth of the N-doped diamond film can be divided into three steps:

(i) forming the nucleation layer

(ii) N-doped diamond film growth

(iii)post treatment.

For the nucleation layer a high sp^2 containing diamond film was grown until the reflected laser signal showed a decrease in its intensity indicating nucleation of the carbon rich film. The growth conditions for the nucleation layer were 400sccm H_2, 8sccm CH_4, chamber pressure of 20 Torr, substrate temperature of 740ºC and a microwave power of 600W.

After deposition of the nucleation layer the flow rates of the process gases were changed to 437sccm H_2, 2.5sccm CH_4 and 60sccm for N_2. The growth temperature was increased to 775ºC and the chamber pressure increased to 50 Torr, the microwave power was increased to 1300W. By using LRI a growth rate of about 0.125μm/hour was determined for this film with an N/C ratio of 48. By growing for 4 to 8 hours, films with thicknesses of 0.5μm and 1μm were fabricated. Growth was terminated by shutting off gas flows except H_2, reducing the microwave power to 600W, and reducing the substrate temperature to 740C.

The last step of diamond film growth was hydrogen passivation with an H_2 Plasma. The microwave power was decreased to 600W, and the chamber pressure was reduced to 20 Torr. The hydrogen passivation process maintained 5 minutes, after which the gas flow was shut off and the sample cooled.

Undoped nanocrystalline diamond films were prepared in the same CVD reactor. The growth conditions for the intrinsic nanocrystalline diamond films were 180 sccm H_2, 20 sccm CH_4, chamber pressure of 20 Torr, substrate temperature of 900ºC and a microwave power of 900 W. Formation of a nucleation layer was not necessary for the nanocrystalline diamond film growth. The growth was terminated after the in situ LRI

monitor showed the desired film thickness. We did not repeat the hydrogen termination step that was described for the N-doped diamond film.

The sulfur doped nanocrystalline diamond films were prepared by hot filament CVD (HFCVD) on polished Mo substrates, and the procedures are described in detail elsewhere. [12]

Characterization of the electron emission from the diamond films was completed by photoelectron emission microscopy (PEEM), field electron emission microscopy (FEEM) and thermionic field electron emission microscopy (T-FEEM).

Our system is an ELMITEC UHV PEEM with a lateral resolution of less than 10nm. [13] The field of view can be changed from 2μm to 150μm, allowing magnifications up to 50.000x. The base pressure in the PEEM main chamber is less than $1x10^{-10}$Torr. For all PEEM, FEEM and T-FEEM studies a voltage of 20,000V was applied between the anode and the sample, over a distance of 4mm. PEEM images were obtained using an Hg-arc lamp as the UV-light source. For FEEM and T-FEEM measurements, the light source was not employed. T-FEEM studies were conducted by radiatively heating of the diamond film and observing electron emission from the sample surface. The temperature of the diamond film was controlled by a thermocouple and optical pyrometer.

Raman scattering was employed to obtain results on the crystal quality and the distribution and concentration of sp^2 and sp^3 bonded carbon. All Raman measurements were conducted at room temperature under ambient conditions using 514.5nm excitation.

In this work we present results of N-doped and B-doped diamond films and undoped and S-doped nanocrystalline diamond films studied by PEEM, FEEM and T-FEEM.

Diamond and nanocrystalline diamond films exhibit electron emission that is significantly different in its nature. The crucial point is uniform versus localized emission which is observed for diamond and nanocrystalline diamond films, respectively. The origin of this emission behavior is still widely discussed and not entirely clear. There is agreement that field enhancement plays an important role in the characteristics for samples with localized emission. However, the electronic structure has often been neglected, where models have attempted to explain the emission mainly by surface morphology.

III. Results and Discussion

We have investigated both, B- and N-doped diamond films. Both were studied with emphasis on thermionic emission properties. The goal was to produce diamond films that display a uniform high electron emission at low temperatures over the whole surface area.

We consider first the results of N-doped diamond films that have been grown with a nitrogen/carbon ratio of 0.5 in the gas phase (N/C = 0.5). These films show the typical diamond surface structure typical of diamond films; small microcrystalls with a size of about 1 micron. AFM measurements reveal a polycrystalline surface with small crystals uniformly distributed over the whole substrate area. PEEM measurements obtained with UV light from a mercury arc lamp show the same surface topography as do AFM measurements and typical images are compared in Figure 1. As mentioned above the crystal edges show higher electron emission due to field enhancement at these sharp crystal boundaries. We also see that the electron emission from this low N-doped diamond film with N/C = 0.5 at room temperature shows a uniform electron emission over the whole surface when irradiated with UV light. By turning off the UV light source the electrons should only be released into vacuum by field emission. Low N-doped diamond films however do not display detectable field emission at room temperature. The next step in our investigation is to study if thermionic field emission occurs (T-FEEM). Increasing the temperature of the low N-doped diamond film does not show electron emission, suggesting that too few N donor states are incorporated into the

diamond lattice and thus the number of electrons promoted into the conduction band lies below our detectable limit.

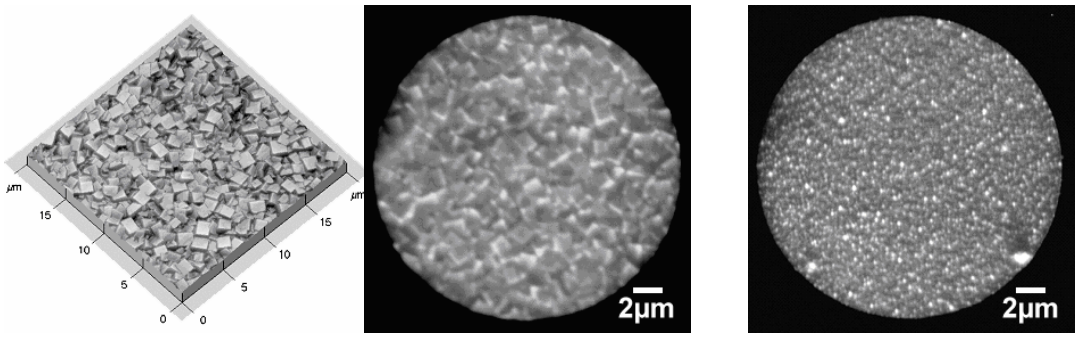

Figure 1 *AFM (left) and PEEM (middle) image of a nitrogen doped diamond film with N/C=0.5. The right image shows a PEEM image of nitrogen doped diamond film with N/C=40. The field of view for the images is 20µm.*

In order to increase the N donor states we have increased the N/C ratio in the gas phase to 48 which we established to be the upper limit for which deposition can be obtained in our system. Above the N/C ratio of 48, the film growth is reduced. With the increased N in the gas phase the surface topography of the diamond films changes significantly. From a microcrystalline morphology for low N-doped diamond films, the structure shifts to a topography characterized by round shaped grains. This structural change is accompanied by a change in the Raman spectrum.

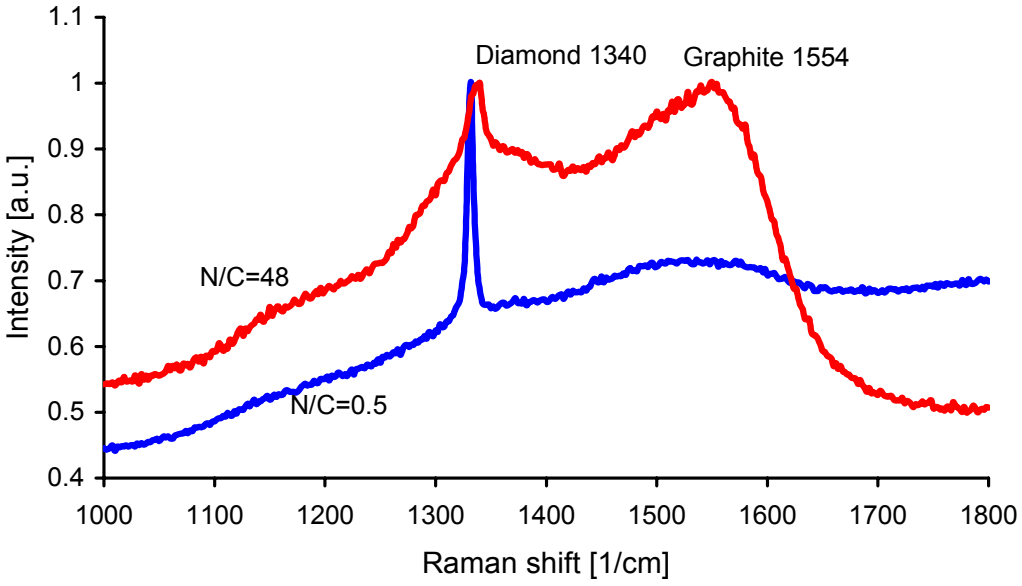

Figure 1.1 *Raman spectra of nitrogen doped diamond films with N/C=48 and N/C=0.5 showing a broadened diamond peak and spectral components attributed to* sp^2 *bonding particularly for the diamond film with higher nitrogen concentration.*

The sharp diamond peak that has been seen for low N-doped diamond is now broadened, and additionally, the peak that corresponds to the sp^2 bonded carbon becomes more pronounced. Raman spectroscopy is able to distinguish between various carbon structures like diamond, graphite, amorphous carbon and hydrogenated carbon. It must be mentioned that from the Raman peak intensity no conclusion has been drawn regarding the fraction of sp^3 and sp^2 bonded carbon because of different sensitivities for different bond structures. In Figure 1.1 the Raman spectrum is shown for an N-doped diamond film with N/C=0.5 and N/C=48. As for the low N-doped diamond film this highly N-doped diamond film was also investigated by PEEM. The image in Figure 1 shows the electron emission from the surface when irradiated with UV light. Compared to the low

N-doped diamond film we observe the change in the surface structure but we still obtain uniform electron emission over the whole surface area. Thus, we do not see any change in the electron emission at room temperature under PEEM for low and high N-doped diamond films.

In the case of field emission we do not find any significant change for either doping type. The electron emission from the highly N-doped diamond film can not be resolved as is the case for the low N-doped diamond film.

From T-FEEM measurements however, we would expect a significant change in the electron emission if we had a high number of N donor states from which electrons could be promoted into the conduction band by thermal energy. The large increase in the electrical conductivity as the temperature is increased is another characteristic of diamond that would also play a crucial role in causing electron transport from the substrate through the N-doped diamond into the vacuum. It has been shown that the electrical conductivity in diamond can vary by 13 orders of magnitude in the temperature range between 100˚C to 1200˚C. [14] This behavior has been attributed to the temperature dependence of the carrier density and the changes in the mobility of the carriers.

As the temperature of the high N-doped diamond film is increased, electron emission is detected at around 600˚C, and above this threshold temperature the electron emission increases strongly with increasing temperature. This indicates that with higher temperature more and more electrons are promoted from the N-donor states in the high N-doped diamond film into the conduction band with contribution of defect states. Once the electrons are in the conduction band they can easily escape into vacuum because of

the NEA surface of the hydrogen passivated diamond film. With increased temperature the Fermi-Dirac distribution changes, so that more electrons are promoted into the conduction band suggesting a strong thermionic contribution to the electron emission.

Introducing nitrogen during the growth process also generates defect states within the diamond in addition to an increase in the sp^2 carbon concentration as it can be determined by Raman spectroscopy. In the Raman spectrum, diamond bonded carbon has a characteristic peak at ~1332cm^{-1}. The FWHM of this peak is related to the inverse of the phonon lifetime and thus sensitive to film disorders. These include grain boundaries, impurities, defects, and amorphous and graphitic phases. Graphitic phases have characteristic peaks between 1575cm^{-1} and 1580cm^{-1}. Different types of defects in graphite lead to different bands. A band at 1355 cm^{-1} has been attributed to in-plane defects in graphite and is often accompanied by broadening of the peak at 1580 cm^{-1}. Amorphous, threefold coordinated carbon has its main band at 1550 cm^{-1}. Raman spectroscopy is ~50 times more sensitive to sp^2 bonding than it is to sp^3 bonding when 514.5nm excitation is used. [22]

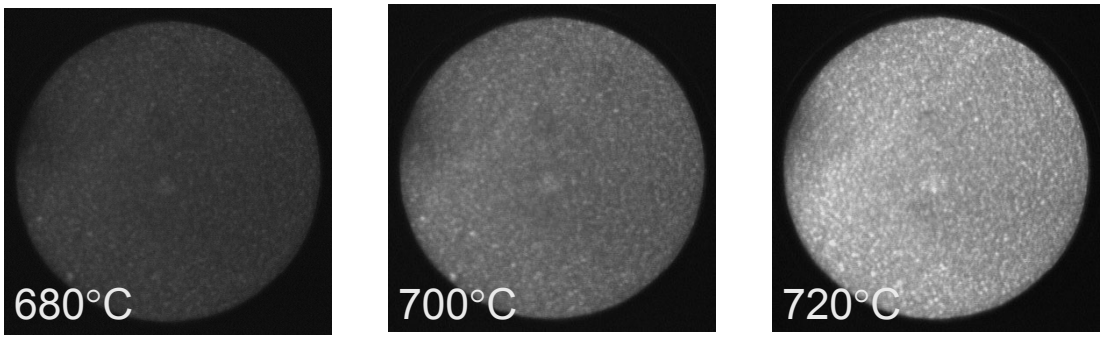

Figure 2 *Thermionic Field Electron Emission (T-FEEM) of nitrogen doped diamond in dependence of temperature. Note the uniform electron emission over the whole surface area. The field of view is 20µm.*

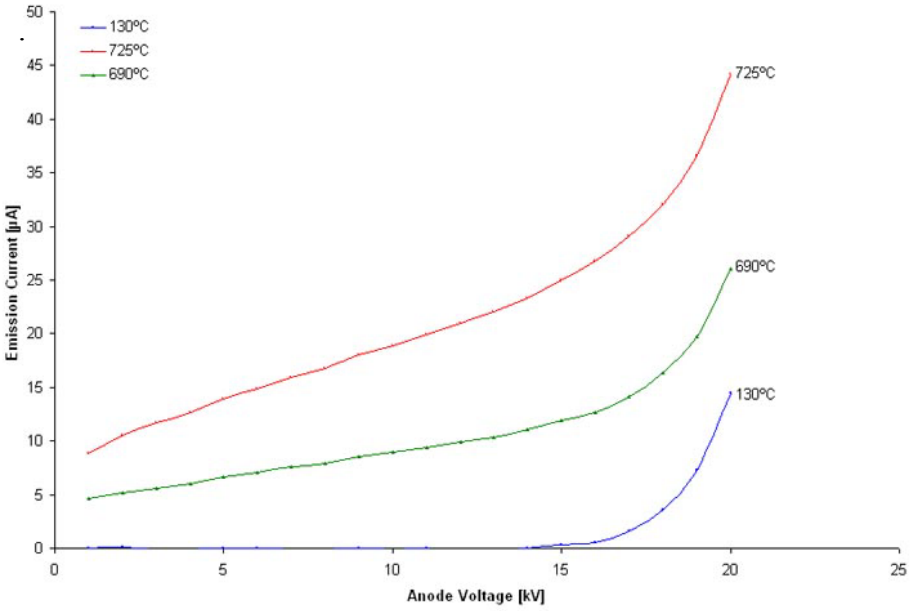

Figure 3 *I/V measurements of N-doped diamond at elevated temperatures.*

Current versus voltage measurements for N-doped diamond show two distinct regions as it is depicted in Figure 3. At low electric fields the emission current is dominated by a relatively field independent component, and at high electric fields an exponential behavior of the electron emission becomes more pronounced. We suggest that the low field emission is due to thermionic processes and the high field emission is due to tunneling. The NEA surface characteristic is of crucial importance for the electron emission to occur. The corresponding sample in Figure 3 was treated with hydrogen plasma to induce a hydrogen passivation layer that results in a negative electron affinity of the diamond surface. Although this H-passivation layer is effective in inducing an NEA surface, its stability at elevated temperatures diminishes significantly entailing a loss in the emission current as shown in Figure 4.

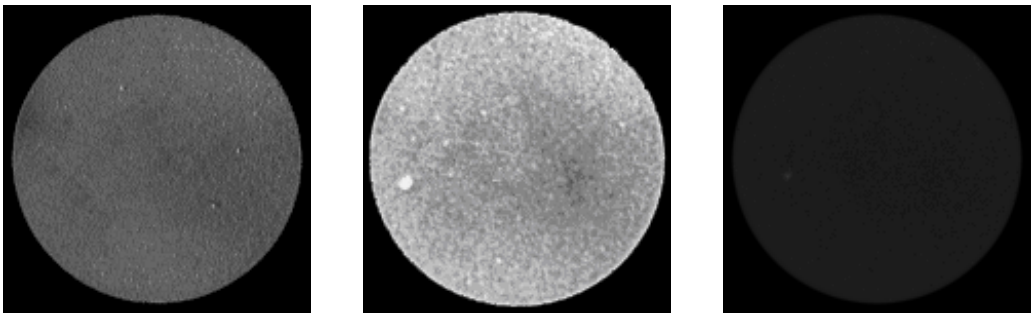

(a) (b) (c)

Figure 4 *Electron emission microscope images (50µm field of view) of H terminated N-doped diamond: (a) PEEM obtained at room temperature with Hg-arc lamp excitation, (b) T-FEEM image at 725ºC at t=0 min and (c) after 10 minutes. The evident decrease in intensity is attributed to the degradation of the hydrogen passivation that induces the NEA.*

The hydrogen passivation layer starts to degrade at a significant rate at around 725ºC. After a time period of 10min after reaching 725ºC, the T-FEEM image shows a strong decrease in brightness corresponding to a reduced electron emission current (see Figure 4b, c). To achieve stable electron emission at elevated temperatures, a metal layer can be deposited on top of the diamond film. A thin titanium layer will induce NEA characteristic that exhibit increased stability with respect to a H terminated surface. In Figure 5 a 2µm thick nitrogen doped diamond film was passivated with a 3Å Ti layer. Electron emission occurred up to 925ºC without a loss in the emission current indicating stable performance of the Ti layer.

This temperature dependent emission behavior is changed significantly when boron is used as a dopant. When utilizing boron as an acceptor in diamond, it will gain

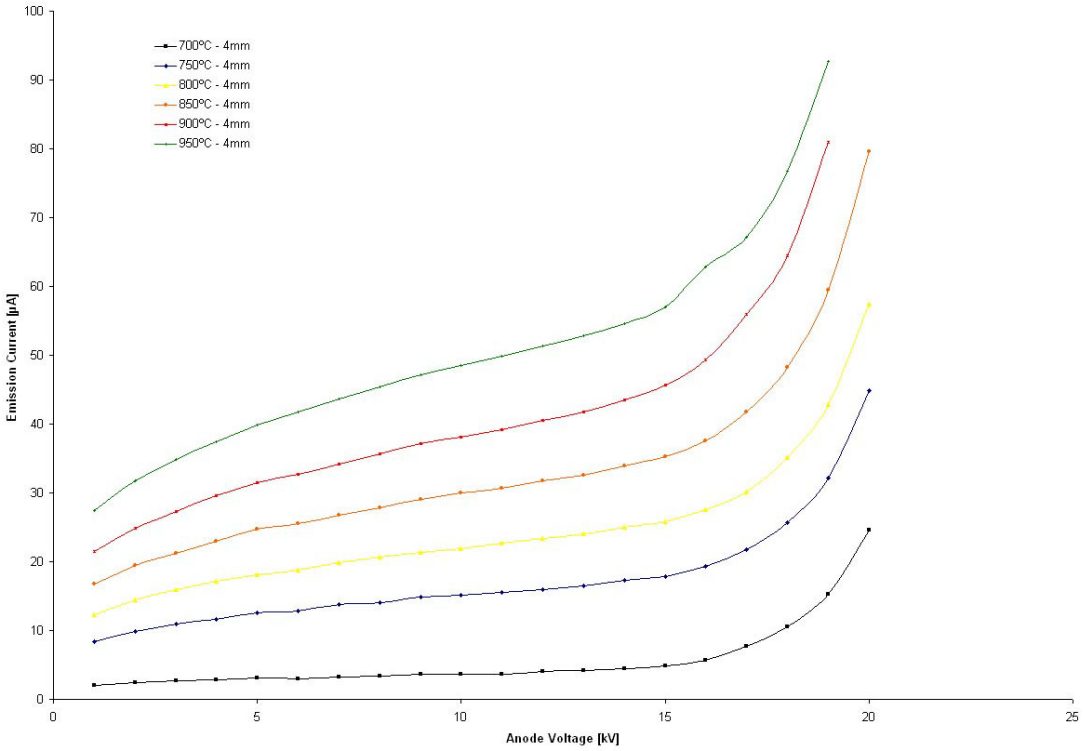

Figure 5 *Thermionic electron emission of a nitrogen doped diamond film with a 3Å Ti passivation layer.*

a p-type characteristic, with the boron states at ~0.33eV above the valence band maximum. Field emission measurements show low electron emission as indicated by field emission microsocopy in Figure 6.

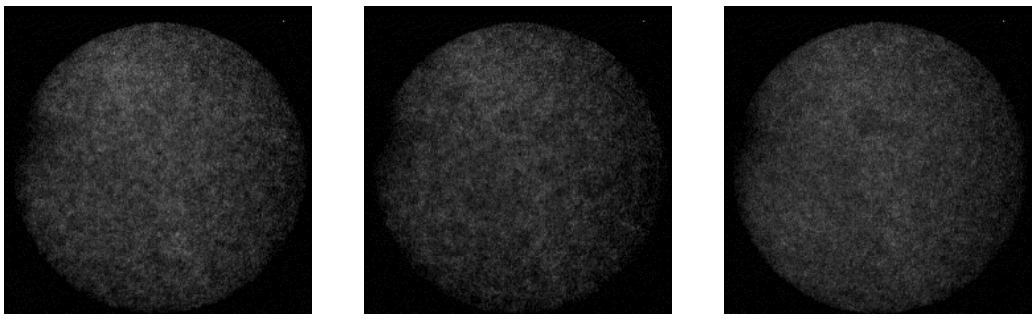

Figure 6 *Field emission microscopy of B-doped diamond (1500ppm) at 640ºC, 680ºC and 800ºC, respectively.*

The B-doped diamond films exhibit low electron emission that remains constant over a wide temperature range. The results show that boron doped diamond films show only weak electron emission at elevated temperatures compared with the highly nitrogen doped diamond films. For the boron doped films we do not observe any significant temperature dependence of the electron emission as we have found for the nitrogen doped films.

While doped or undoped diamond films do not exhibit significant field emission at room temperature, nanocrystalline diamond films have excellent field emission properties in regard to low threshold field and high current densities. The emission structure however differs in a crucial way from that of diamond films as the emission is localized and thus non-uniform. Field emission electron microscopy can be employed to study the spatial distribution of the electron emission and develop a map relating emission to specific morphology. Figure 7 depicts a FEEM image acquired at an electric field of 5V/μm.

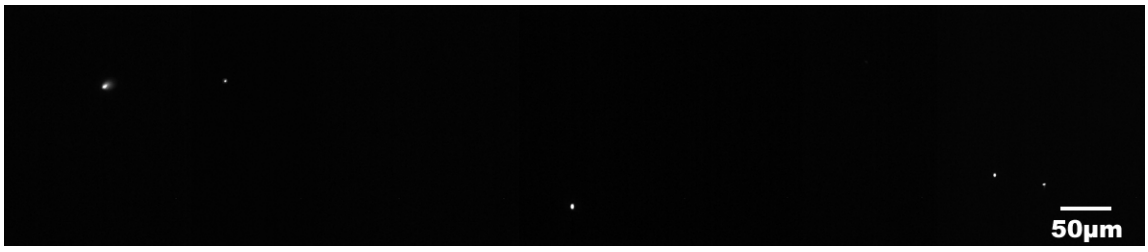

***Figure** 7 Field-electron emission microscopy (FEEM) of a region of intrinsic nanocrystalline diamond showing 5 emission sites.*

Electron emission that is localized in its nature is indicative of a high field enhancement factor β. This suggests a very high localized electric field that allows electrons to tunnel through an otherwise high barrier. With an increase in the local electric field the barrier thickness decreases and more electrons will be released into vacuum resulting in an increased tunneling current. A schematic of how high field enhancement is achieved is shown in Figure 8. Flat, smooth surfaces exhibit a uniform field enhancement with no preferred region for electron emission. Surface features with a high aspect ratio show field enhancement factors up to several 1000's, thus becoming sites for field emission. The high field enhancement leads to a concentration of the electric field and electron emission originated from those preferred structures.

Figure 8 *A flat surface exhibits a uniform low field enhancement factor (left image) while sharp, pointed structures show high field enhancement (right image).*

Field enhancement alone can result in an emission structure as is shown in Figure 7. The origin of the emission spots would then coincide with structural features that have a field enhancement factor high enough to allow significant tunneling of electrons into vacuum. Surface characterization techniques such as scanning electron microscopy and

atomic force microscopy can be employed to investigate the surface morphology to identify specific morphologies that would enable electrons to be released by tunneling processes.

A scanning electron micrograph of a nanocrystalline diamond film is shown in Figure 9. The surface is characterized by a uniform micron and submicron array separated by grain boundaries. Within the detection limit, no significant surface features can be observed that would account for a high field enhancement feature. It has been argued that a specific nanostructure protrusion with a high field enhancement is responsible for the electron emission. [15, 16] Another explanation for the emission behavior is the occurrence of grain boundaries within the film. This network of reportedly high sp^2 carbon could serve as the conducting material in between the insulating sp^3 grains and thus exhibit a high field enhancement that would lead to electron emission due to tunneling. [17] Examining the film morphology shows a high uniformity of the grain boundary network. However, the electron emission map shows a significantly reduced number of emission sites compared to the density of the grain boundaries. Thus, field enhancement alone can not account for the observed emission pattern.

Intrinsic nanocrystalline diamond has been shown to have an emission site density of about 10^4-$10^5 cm^{-2}$. This raises the question on the origin of the electron emission since only 1 in 10,000 sites would emit although the surface morphology does not differ in the same way. This pattern of electron emission is similar to other carbon based materials. Carbon nanotube (CNT) films exhibit an emission site density that is in the same order as that of nanocrystalline diamond although the CNT density is orders of magnitude higher.

This phenomenon emphasizes the question of how electron emission occurs and what makes a site preferred to be an electron emitter.

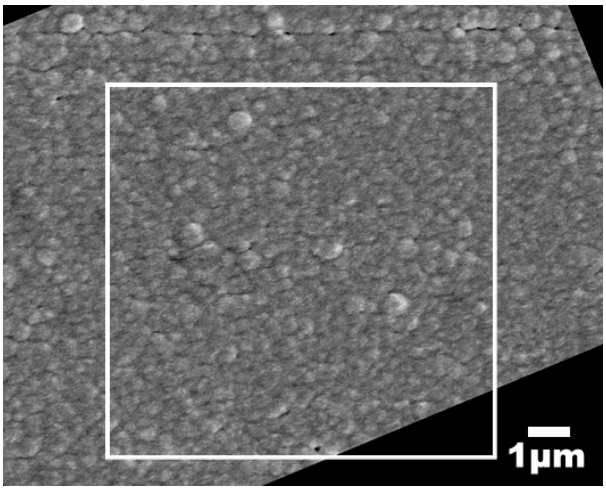

Figure 9 *Scanning electron micrograph of a nanocrystalline diamond film.*

To further investigate morphology of a nanocrystalline diamond sample and the emission behavior mapping of surface features with the spatial distribution of emission sites can be performed. Electron emission microscopy is employed to image the emission sites and the results are correlated to morphology as imaged by SEM.

In Figure 10 PEEM, FEEM and SEM images of the same surface region are displayed. Irradiating the surface of nanocrystalline diamond with UV light from a Hg-arc lamp results in a PEEM image as shown in Figure 10 (a). A bright white spot can be observed and is indicated by the white box. This feature is recognized as an electron emission site. An overlay image consisting of SEM and PEEM as shown in Figure 10 (b) can be utilized to correlate surface morphology with the emission characteristics. Without any light excitation emission is reduced as it is shown in the field emission image

(FEEM) in figure 10 (c). The size of the emission site appears smaller when emission is due only to tunneling. To investigate the surface structure of the emission site area SEM can be employed to acquire a high magnification image which is shown in Figure 10 (d).

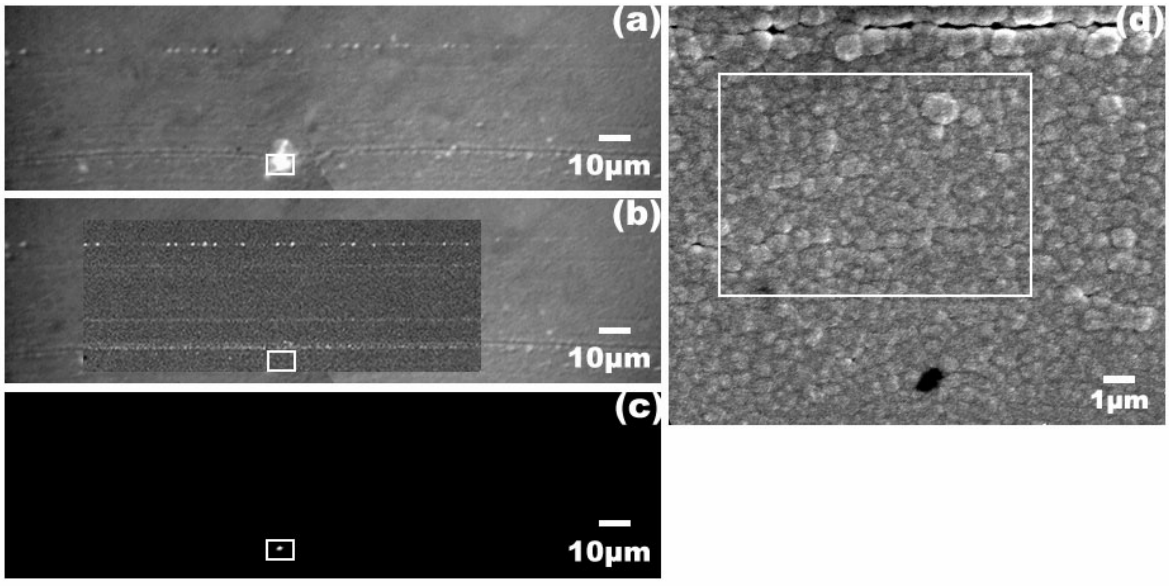

Figure 10 *PEEM, FEEM and SEM images of an electron emission site. (a) PEEM image with the emission site within the white box; (b) front image: SEM back image: PEEM, the white box in the SEM image indicates the region of electron emission; (c) FEEM image of the emission site and (d) SEM image of the surface area where the emission originates (within the white box).*

The surface is characterized by micron and sub-micron grains separated by their corresponding boundaries. Within the white box where the electron emission can be located, no significant change in morphology can be observed, nor do preferred features appear in the SEM micrograph. In fact, there is no region within the indicated area that would differ from any region outside in such a way that would make it preferred for electron emission. These results suggest that surface feature induced field enhancement

can not solely account for the observed emission pattern. The electronic structure of the material under high electric fields is a crucial parameter in field emission.

Field emission per se does not significantly depend on temperature. Thermionic field emission microscopy (T-FEEM) can be utilized to image the temperature dependence of the field emission. The T-FEEM images in Figure 11 do not show a significant change in electron emission with increasing temperature in accordance with the field emission behavior.

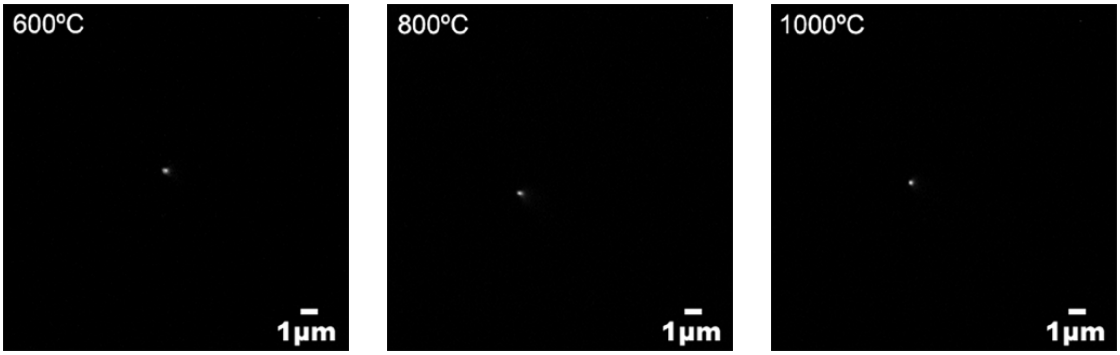

Figure 11 *Thermionic field electron emission microscopy of nanocrystalline diamond films showing no significant increase in electron emission with an increase in temperature.*

However, in Figure 13 the thermionic I/V measurements show a distinct temperature dependence of the electron emission of the intrinsic nanocrystalline diamond. We note that the thermionic I/V measurements employ a large anode, which allows measurement of the emission from many sites. Performing a Fowler–Nordheim analysis of the data by plotting log I vs. 1/V, it can be determined if the emission characteristic exhibits F–N behavior by fitting with a straight line. (Figure 12) Our results

indicate that the electron emission pattern is described by Fowler–Nordheim tunneling. There was no evidence of a thermionic emission component which would be observed at low electric fields, but at increased electric fields the temperature dependence becomes more pronounced.

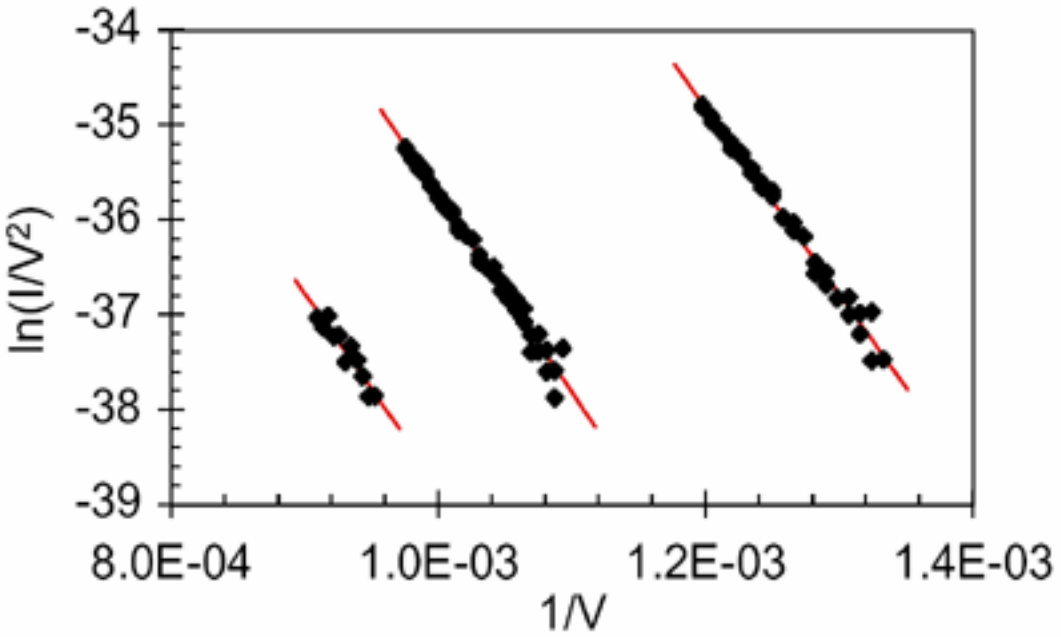

Figure 12 *Fowler-Nordheim plot with data fitted by a straight line.*

Another way to achieve n-type characteristics is through doping with sulfur. Sulfur doping introduces donor states that have been reported to have a theoretical activation energy of 0.375eV below the conduction band minimum. [18, 19] This significant reduction in the activation energy when substituting nitrogen with sulfur should result in a more pronounced thermionic electron emission component at lower temperatures. The sulfur doped nanocrystalline diamond films were prepared by hot

filament CVD on polished Mo substrates, and the procedures are described in detail elsewhere [20].

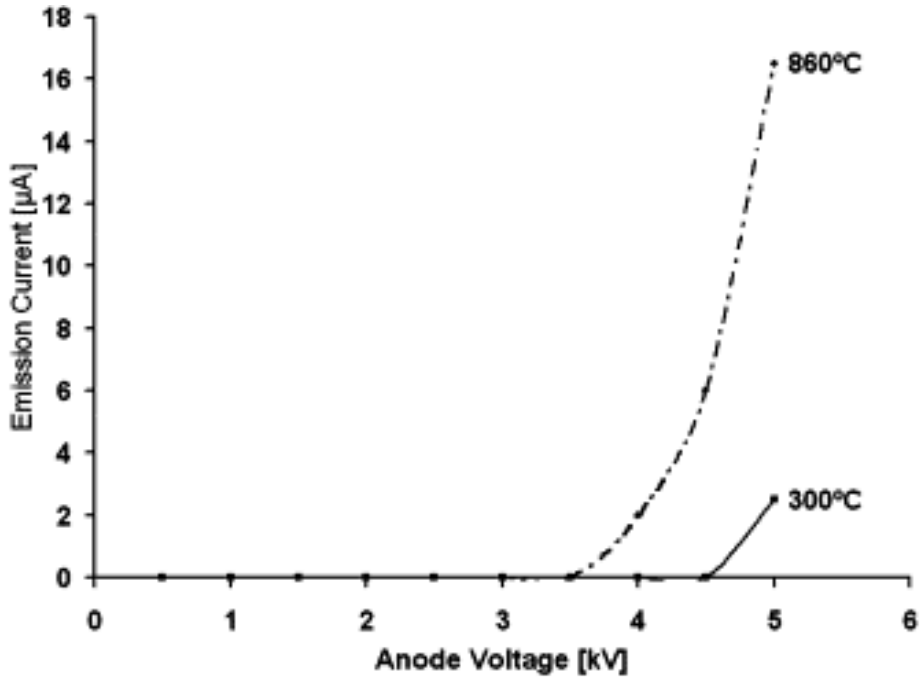

Figure 13 *Thermionic electron emission measurement of undoped nanocrystalline diamond at 300 and 860 °C with a sample-anode spacing of 2 mm.*

Scanning electron measurements of sulfur doped nanocrystalline diamond films show a surface structure that is characterized by small grains significantly smaller than typical grains in undoped nanocrystalline diamond films. (Figure 14) However, as shown in Figure 13, both films exhibit a uniform surface morphology that indicates the presence of small grains presumably separated by conducting, sp^2 graphite containing boundaries [21]. The sulfur doped film apparently exhibits a smaller grain size than the intrinsic nanocrystalline diamond. Grain sizes for the intrinsic films are of the order of ~0.5µm while for the sulfur doped films SEM indicates a grain dimension of ~0.1µm.

Although the surface structure of the sulfur doped films differs from intrinsic nanocrystalline films, the field emission behavior is similar in many aspects. Electron

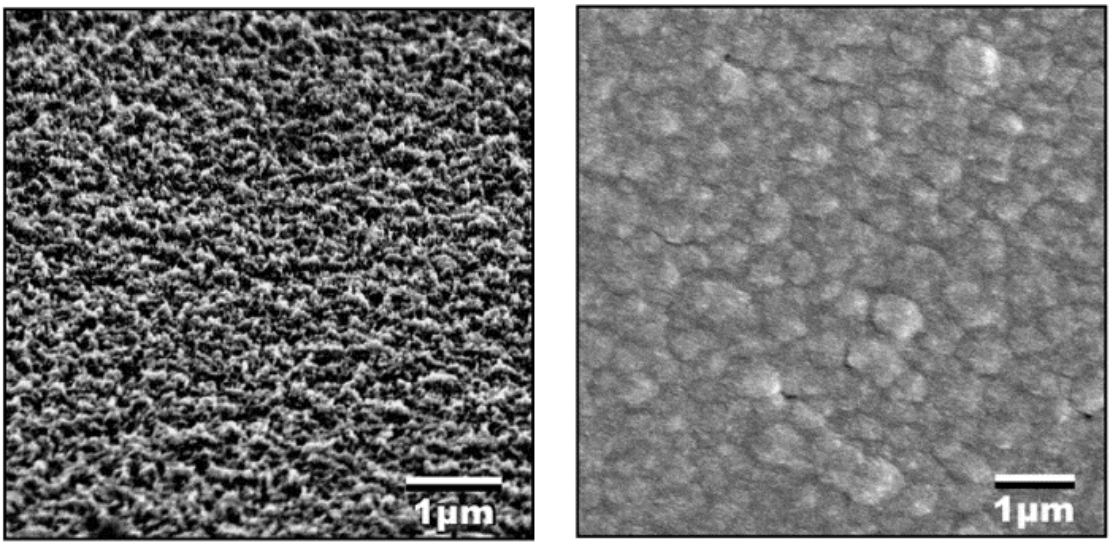

Figure 14 *SEM images of sulfur doped (left) and intrinsic (right) nanocrystalline diamond films.*

emission for sulfur doped films originates from small, localized sites indicating the significance of field enhancement for emission.

Using FEEM, the emission sites can be imaged as is shown in Figure 14. The room temperature emission is essentially the same as that from the intrinsic nanocrystalline diamond films. FEEM was employed to determine the emission site distribution. Figure 7 depicts a large region of the intrinsic nanocrystalline diamond film surface imaged in FEEM mode with five clearly identified emission sites, resulting in an emission site density of approximately $5\times10^3/cm^2$ at an electric field of 5 V/μ.

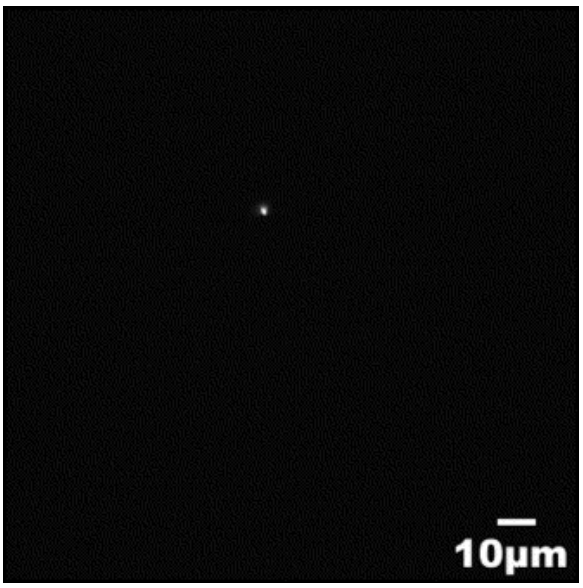

Figure 15 *FEEM of sulfur doped nanocrystalline diamond showing electron emission originating from an emission site.*

Figure 15 displays an emission site of the S-doped film. This film also displayed an emission site density of ~10^4/cm^2. This density is comparable to many prior reports of efficient emitting films. To investigate the temperature dependence of the electron emission, the sample was radiatively heated in the electron emission microscope, and the emission was imaged by the instrument. At elevated temperatures the electron emission increases significantly as it is shown in Figure 16. The thermionic I/V measurements shown in Figure 17 clearly indicate a thermionic component of the emission current that can be observed at low electric fields. At temperatures below 170°C, an electron emission current cannot be detected at electric fields smaller than ~2.25V/µm**.** However as the temperature is increased significant electron emission is observed which is attributed to thermally excited electrons.

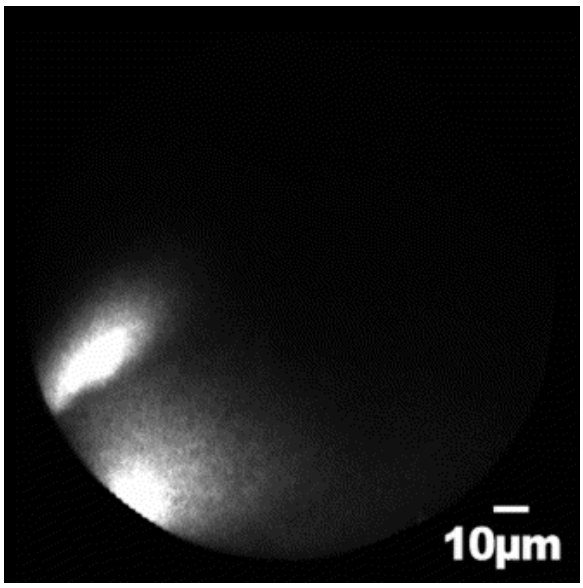

Figure 16 *T-FEEM of sulfur doped nanocrystalline diamond showing increased electron emission originating from localized regions.*

In addition, I/V curves at higher electric fields display a strong contribution characteristic of a tunneling current. Comparing the emission behavior of intrinsic and sulfur doped nanocrystalline diamond films strongly suggests that sulfur donor states supply carriers that can be released into vacuum when thermal energy is supplied. The results show that doped diamond and doped nanocrystalline diamond both exhibit a thermionic component to the emission current. For nitrogen doped diamond films emission is uniform suggesting thermally excited electrons are released into vacuum from the conduction band. Emission behavior for sulfur doped nanocrystalline diamond films differs in a way that at elevated temperatures emission is not uniform but occurs from the same emission sites that exhibit field emission at room temperature.

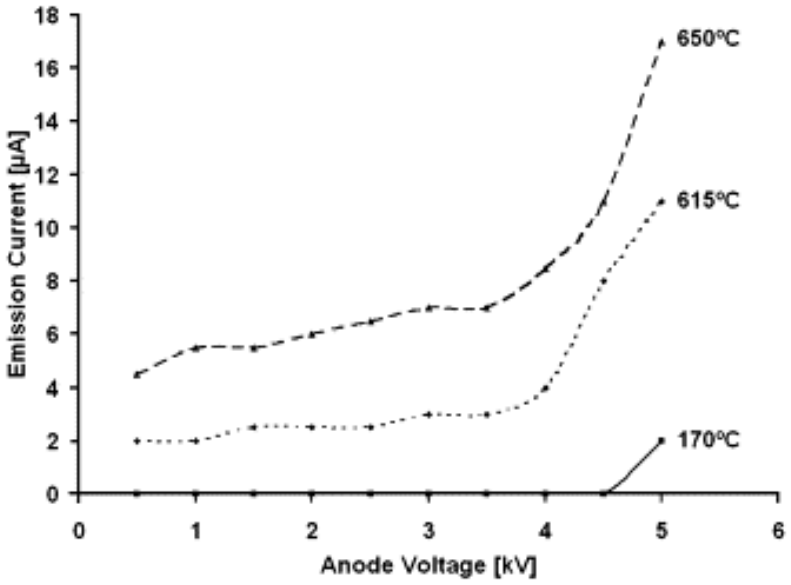

Figure 17 *Thermionic electron emission measurement of sulfur doped nanocrystalline diamond at various temperatures.*

A schematic band diagram for electron emission from nitrogen doped diamond films is shown in Figure 18. The nitrogen donor states are indicated by [N]. Defect states within the film are illustrated by [D]. Since nitrogen doped diamond films can gain a negative electron affinity the surface barrier vanishes. Nitrogen doped diamond exhibits upward band bending, and the applied high electric field will penetrate the film surface as is shown in Figure 18. From the band structure in Figure 18, it is evident that the total emission current can be composed of several components. One results from thermally excited electrons from the nitrogen states. These electrons, which have been promoted into the conduction band, are released into vacuum because of the NEA surface. At high electric fields tunneling can occur from other states within the film. With an increase in

the applied voltage the field emission component should become more pronounced, where defect states in the film can also act as a source for electron emission. A suitable combination of defect states would allow hopping mechanism, providing a path for carriers into the conduction band or to defect states slightly below the conduction band, where carriers can tunnel through a diminished barrier.

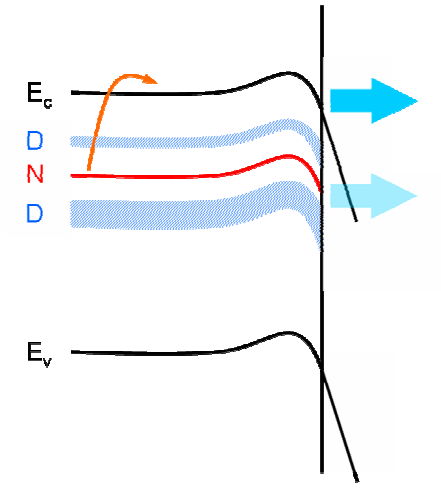

Figure 18 *Schematic band structure of nitrogen doped diamond showing enhanced electron emission at elevated temperatures due to ionized N donor states. (The location and width of the defect-induced states D are for illustration only.)*

As is shown in Figure 18, electrons promoted into the conduction band can be released into vacuum due to the NEA surface that reduces the vacuum level to below the conduction band minimum. Undoped nanocrystalline diamond films exhibit a different band structure which is shown in the schematic in Figure 19. Electron emission for nanocrystalline diamond films can be explained in terms of a high field enhancement factor β. This corresponds to a steep slope of the field line on the vacuum side in Figure 19 which is defined in Fowler-Nordheim tunneling. Defect [D] states within the film can

contribute to the total emission current if electrons can tunnel through the barrier. Introducing shallow donor states [S] should lead to a change in electron emission at elevated temperatures. If the donor states are located at a certain depth, they should not alter the electron emission since carriers could not tunnel through a still large barrier.

In order for electrons from donor states to contribute to the electron emission, they would have to occupy states near the surface emission sites from which tunneling can occur. Promoting electrons from these donors by thermal excitation would then significantly increase the overall emission current. Temperature dependent electron emission is not only determined by suitable donors within the film but also by the electrical conductivity of the material i.e. diamond.

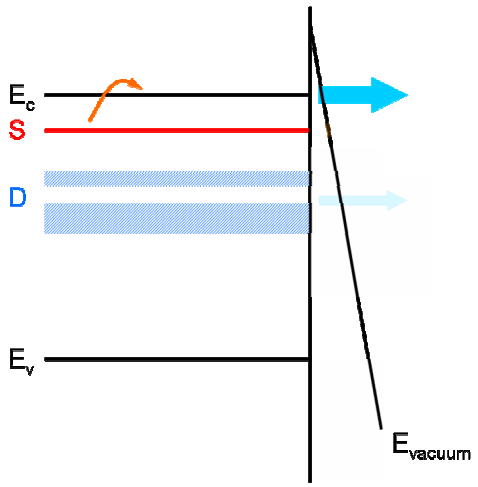

Figure 19 *Schematic band structure of nanocrystalline diamond where electron emission is due to Fowler-Nordheim tunneling. Donor states [S] lead to an increase in electron emission at elevated temperatures. (The location and width of the defect-induced states D are for illustration only.)*

With increasing temperature the electrical conductivity exhibits a significant increase from ~$10^{-14}\Omega^{-1}cm^{-1}$ to ~$10^{-7}\Omega^{-1}cm^{-1}$ when the temperature is increased from 200ºC to 800ºC. This increase is attributed to carrier density temperature dependence and change in the carrier mobility. [22] In order to study this electron emission we begin by examining electron emission from a metal.

The following discussion is a summary from *Field, Thermionic, and Secondary Electron Emission Spectroscopy* and can be found in more detail in reference [23]. The model involves a semi-infinite metal that has been chosen to extend from $z = -\infty$ to $z = 0$. Electrons within this metal see a constant (zero) potential and can be considered to be free. For an electron to escape the metal, it has to be supplied with energy equal to the work function ϕ. It is well known that an electron outside a metal sees an image charge that results in an image force

$$\frac{-e^2}{4z^2}.$$

The potential energy of the electron is then given by

$$V(z) = E_F + \phi - \frac{e^2}{4z^2},$$

which changes under the influence of an electric field F to

$$V(z) = E_F + \phi - \frac{e^2}{4z^2} - eFz \, .$$

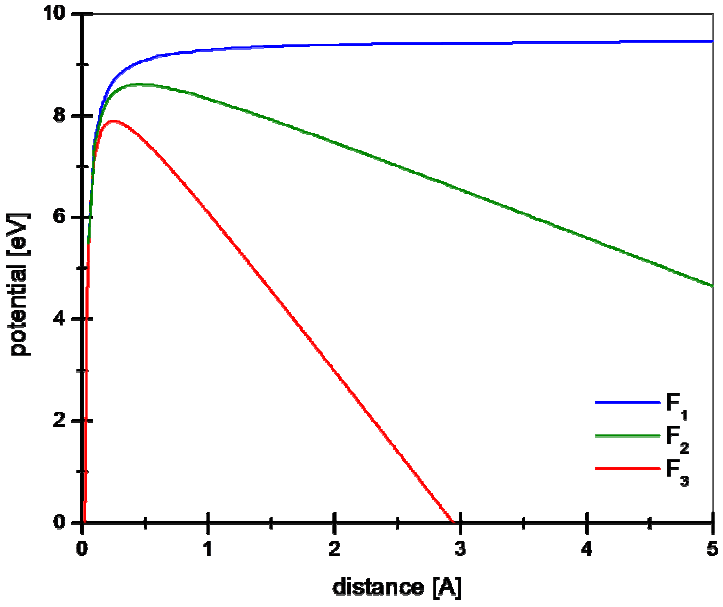

Figure 20 *Surface potential barrier for an electron at increasing electric fields F_1, F_2 and F_3 where $F_1 < F_2 < F_3$.*

An electron at the vacuum side will see a surface potential barrier that is reduced as the electric field is increased (Figure 20). If $D(W)$ is the probability for an electron to tunnel through the barrier and $N(W,T)$ the number of electrons available then the emission current density can be written as

$$J(F,T) = e\int_0^\infty N(W,T)\cdot D(W,T)dW \, .$$

The transmission coefficient $D(W)$ is given by

$$D(W) = \left\{1 + e^{-A(W)}\right\}^{-1}$$

where

$$A(W) = 2i\int \left\{\frac{2m}{\hbar^2}\left[W - V(\wp)\right]\right\}^{\frac{1}{2}} d\wp \,.$$

As has been shown in detail elsewhere [23], the general expression for the current density can be written as

$$J(F,T) = e\int_0^\infty N(W,T)\cdot D(W,T)dW$$

$$= \frac{emk_BT}{2\hbar^3\pi^2}\left\{\int \frac{\ln\left(1+e^{\frac{-(W-E_F)}{k_BT}}\right)}{1+e^{A(W)}}dW + \int \ln\left[1+e^{\frac{-(W-E_F)}{k_BT}}\right]dW\right\}$$

In the case of field emission, $\exp\left[A(W)\right] >> 1$ and we can write

$$J(F,T) = \frac{emk_BT}{2\hbar^3\pi^2}\int e^{-A(W)} \ln\left[1+e^{\frac{-(W-E_F)}{k_BT}}\right]dW$$

Expanding the exponent of the transmission coefficient in a Taylor series around E_F

$$-A(W) = -b_0 + c_0(W - E_F) - f_0(W - E_F)^2 + \ldots$$

with

$$b_0 = 0.683v\left(3.79\frac{F^{1/2}}{\phi}\right)\frac{\phi^{3/2}}{F}$$

$$c_0 = 1.025v\frac{\phi^{1/2}}{F}t\frac{3.79F^{1/2}}{\phi}$$

$$f_0 = 0.256\frac{1}{F\phi^{1/2}}v\frac{3.79F^{1/2}}{\phi}\frac{1}{1-\dfrac{14.36F}{\phi^2}}$$

where

$$t(y) \equiv v(y) - \frac{2}{3}y\frac{dv}{dy}$$

and

$$y_0 = 3.79\frac{F^{1/2}}{\phi}.$$

Substituting gives

$$J(F,T) = \frac{emk_BT}{2\hbar^3\pi^2}e^{-b_0}\int e^{c_0(W-E_F)}\ln\left[1+e^{\frac{-(W-E_F)}{k_BT}}\right]dW$$

which can be evaluated as

$$J(F,T) = \frac{e^3F^2}{16\pi^2\hbar\phi t^2(y_0)}\frac{\pi c_0k_BT}{\sin(\pi c_0k_BT)}\exp\left[-\frac{4}{3e}\left(\frac{2m}{\hbar^2}\right)^{1/2}v(y_0)\frac{\phi^{3/2}}{F}\right]$$

At low temperatures, i.e. when $\pi c_0 k_B T << 1$ the above dependence corresponds to the Fowler-Nordheim equation

$$J(F) = A' F^2 e^{\frac{-B'\phi^{3/2}}{F}}$$

where

$$A' = \frac{e^3}{16\pi^2 \hbar \phi t^2 \left(\frac{\sqrt{e^3 F}}{\phi} \right)}$$

and

$$B' = \frac{4}{3e} \left(\frac{2m}{\hbar^2} \right)^{1/2} v\left(\frac{\left(e^3 F\right)^{1/2}}{\phi} \right).$$

A substitution leads to

$$J(F) = \frac{1.537 \times 10^{10} F^2}{\phi t^2 \left(3.79 F^{1/2} / \phi\right)} \exp\left[-\frac{0.683 \phi^{3/2}}{F} v\left(\frac{3.79 F^{1/2}}{\phi} \right) \right] \frac{A}{cm^2},$$

where ϕ is given in eV and F in $V/\text{Å}$. From this it is found that if $\ln\left(J/F^2\right)$ versus $1/F$ is plotted, it results in a straight line for a typical field emission experiment, and from the slope of the line the work function can be obtained.

At high temperature and under weak applied electric fields, the current density is described by

$$J(F,T) = \frac{em(k_B T)^2}{2\pi\hbar^3} \frac{\pi h_0}{\sin \pi h_0} \exp\left[-\frac{\phi - (e^3 F)^{1/2}}{k_B T} \right]$$

where

$$h_0 \equiv \left(\frac{F\hbar^4}{m^2 e^5} \right)^{1/4} \frac{(e^3 F)^{1/2}}{\pi k_B T} .$$

In case of very weak applied fields this reduces to

$$J(F,T) = A_R T^2 \exp\left[-\frac{\phi - (e^3 F)^{1/2}}{k_B T} \right]$$

where

$$A_R = \frac{emk_B^{\ 2}}{2\pi^2\hbar^3} = 120 A cm^{-2} K^{-2}$$

which is the well known Schottky formula. A plot of the Schottky formula is shown in Figure 21. The formula is plotted in dependence of the temperature showing an increase of the emission current with increasing temperature and an increase of the electron emission when the electric field is increased from F_1 to F_2. If the electric field F is set to *0* the Schottky equation becomes the Richardson-Laue-Dusham equation.

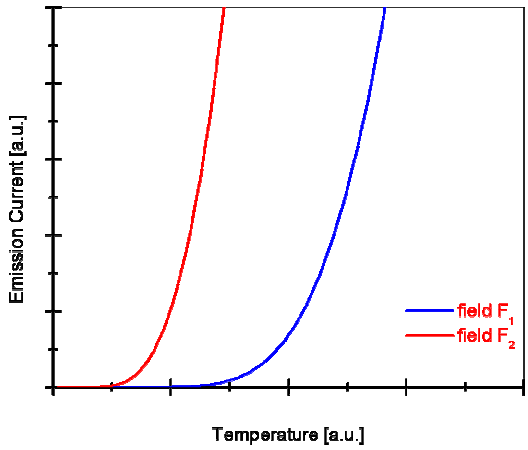

Figure 21 *Plot of the Schottky formula in dependence of the temperature at various electric fields F_1 and F_2, where $F_2>F_1$.*

Electron emission presented in this study, especially emission from intrinsic and sulfur doped nanocrystalline diamond should be described by a combination of field emission and thermionic emission. Sulfur doped nanocrystalline diamond has been shown to exhibit significant electron emission at fields of about 5V/µm and at temperatures of about 600ºC. The electric field mentioned here is the macroscopic field calculated form the voltage applied between sample and anode separated by a certain distance.

Electron emission micrographs indicate whether the macroscopic field can be considered as the actual field at the location of the emission. It has been found that the electric field at a tip surface can be described by

$$F = \beta \cdot V$$

where β is termed as field enhancement factor indicating that the local field at the emission site can be considerably larger. Field emitting structures like tips with a high aspect ratio can have field enhancement factors of several 1000's. Additionally, it can not be assumed that under high electric fields the field emitter shows the same electronic structures as in equilibrium thus being different from field emission as it was described for metals. Semiconductors in general experience field penetration which leads to band bending at the surface and significant changes of the electronic structure.

Similar to the case of a semi-infinite metal we now consider a semi-infinite semiconductor that extends from $z = -\infty$ to $z = 0$. An applied electric field has its component normal to the surface and has a value F_0. The band bending due to the applied electric field is shown schematically in Figure 22. The fields at the conduction band minimum and valence band maximum are denoted by E_c and E_v, respectively. With band bending occurring the density of states can be described by

$$\rho(E,z) \cong \rho_\infty(E - E_c(z))$$

where $\rho_\infty(E)$ is the density of states in the unperturbed region of the semiconductor measured from the bottom of the conduction band. The density of states in the surface region, that usually is only a few atomic layers thick, is generally different from the bulk density of states. In the space charge region the above equation can be considered valid due to the fact that the field penetrating the semiconductor varies slowly

with depth so that it can be approximated as a constant function over a distance of the order of the lattice constant.

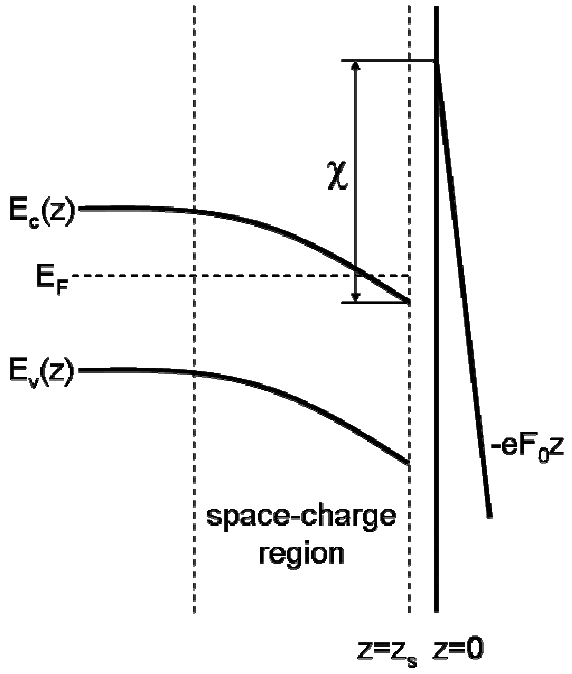

Figure 22 *Field penetration causes band bending near a semiconductor surface.*

The constant Fermi level corresponds to an equilibrium Fermi-Dirac distribution of electrons within the semiconductor. This is true in the limit of small emitted currents and is termed the zero-emitted-current approximation. In this case the current flowing through the sample can be neglected.

The concentration of electrons n(z) in the conduction band and holes p(z) in the valence band is given by

$$n(z) = \int_{E_c(z)}^{\infty} \rho_{\infty}(E - E_c(z)) f(E) dE$$

$$p(z) = \int_{-\infty}^{E_c(z)-E_g} \rho_\infty (E - E_c(z))[1 - f(E)]dE$$

where $f(E)$ is given by the Fermi-Dirac distribution function and $E_g = E_c(z) - E_v(z)$ is the band gap. The concentration for ionized donors $N_d^+(z)$ and for ionized acceptors $N_a^-(z)$ can be written as

$$N_d^+(z) = N_d \left\{ 1 + 2\exp\left[\frac{E_F - E_c(z) - \varepsilon_d}{k_B T} \right] \right\}^{-1}$$

$$N_a^-(z) = N_a \left\{ 1 + 2\exp\left[-\frac{E_F - E_c(z) - \varepsilon_a}{k_B T} \right] \right\}^{-1}$$

with N_d and N_a the concentrations of donors and acceptors, respectively, and the energy levels are given by ε_d and ε_a. It is well known that

$$\rho_\infty (E - E_c) \cong \frac{1}{2\pi^2} \left(\frac{2m_n}{\hbar^2} \right)^{3/2} (E - E_c)^{1/2}$$
$$\cong \frac{1}{2\pi^2} \left(\frac{2m_p}{\hbar^2} \right)^{3/2} (E_c - E_g - E)^{1/2}$$

where m_n and m_p are the effective masses for electrons and holes, respectively. These carriers will play an important role in case of thermionic emission since donor states are introduced into the semiconductor with the purpose of providing carriers which

can be promoted into the conduction band at moderate temperatures where they can be released into vacuum.

A band schematic is shown in Figure 23 for the zero-current-approximation for a n-type semiconductor, where there is no voltage drop within the semiconductor. In this case the bands exhibit upward band bending with a negative $\Delta E_c = E_c(-\infty) - E_c(z_x)$ in order to account for the charge in the surface band indicated by the shaded region.

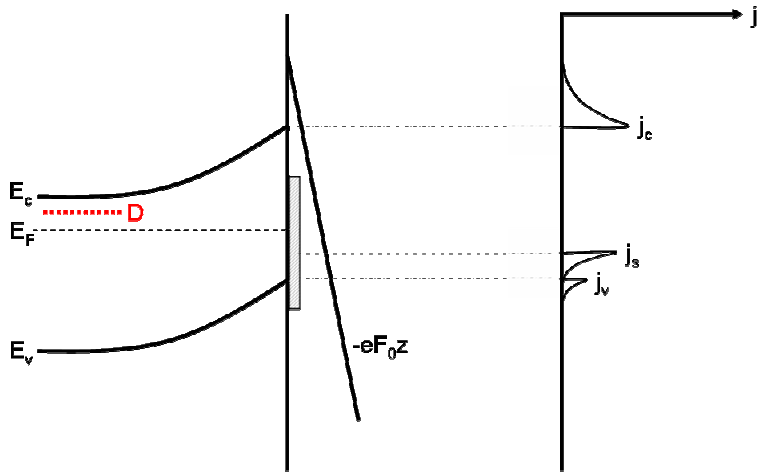

Figure 23 *Schematic band diagram for a n-type semiconductor under an electric field F_0 and the contributions to the total emission current j. Donor states are symbolized by D.*

If donors are introduced they will form states *D,* which can be ionized by thermal excitation thus providing additional electrons for emission. This makes clear that doping itself does not alter field emission behavior at room temperature consistent with our observations for sulfur-doped nanocrystalline diamond. However, at elevated temperatures donors play an important role resulting in an increase of the overall emission current. Ionized donors will supply electrons that can be released into vacuum through the existing emission sites. From experiment and the band diagram in Figure 23

it can be seen that a thermionic emission component, i.e. emission at low electric fields has a low probability. A thermionic component would be detected if electrons would have sufficient energy to overcome the surface barrier, and this would result in a uniform electron emission throughout the surface area of the semiconductor. This would be detected as a uniform emission intensity image in the electron emission microscope; as is the case for nitrogen doped diamond films.

The thermionic component that has been observed for nitrogen-doped diamond films can be detected at very low electric fields excluding any field emission component due to tunneling. We suggest that nitrogen donor states ionized at higher temperatures release electrons into the conduction band with a carrier concentration that increases with increasing temperature similar to a typical thermionic emitter. Due to the absence of a surface barrier, because of the presence of the NEA surface, these electrons can be removed from the semiconductor by even small electric fields. The exact band structure may include defect states that influence the total emission current.

IV. Conclusion

Thermionic electron emission of nitrogen-doped diamond, intrinsic nanocrystalline diamond and sulfur-doped diamond has similarities in their nature that can be explained by a physics based model of the materials and emission process.

In my studies electron emission microscopy has been employed to investigate emission behavior of these materials focusing on the dependence of the applied electric field and temperature. Nitrogen-doped diamond does not exhibit significant field emission at room temperature due to the lack of suitable states within the film. However, at elevated temperatures nitrogen donor states become ionized supplying electrons that are promoted into the conduction band or to nearby defect states. The ability of diamond surfaces to gain a negative electron affinity results in the absence of a surface barrier, i.e. the vacuum level is reduced to below the conduction band minimum. Electrons from nitrogen donors that are promoted into the conduction band can thus be removed by even small electric fields. Electron emission microscopy detects this form of emission as bright, uniformly emitting surfaces that show an increase in brightness with increasing temperature.

Intrinsic nanocrystalline diamond exhibits electron emission that is confined to emission sites which appear as small bright spots in the electron emission microscope images. This emission behavior can be explained by field emission due to tunneling through a barrier. The local electric field of the emission can be assumed to be increased by the field enhancement factor β. Field emission at elevated temperatures for intrinsic nanocrystalline diamond does not exhibit a significant change in electron emission in

accordance with the band structure. Introducing shallow donors can be ionized at moderate temperatures. This can be accomplished by doping with sulfur. Electrons from thermally excited sulfur atoms can be released into vacuum by tunneling from the existing emission sites. The high surface barrier for nanocrystalline diamond films does not allow emission over this barrier at moderate temperatures.

Thus I have developed a consistent model of thermionic emission from diamond films which accounts for the uniform emission of N-doped films and the intense site emission from S-doped nanocrystalline diamond films.

References

(1) A. R. Krauss, O. Auciello, D. M. Gruen, A. Jayatissa, A. Sumant, J. Tucek, D. C. Mancini, N. Moldovan, A. Erdemir, D. Ersoy, M. N. Gardos, H. G. Busmann, E. M. Meyer and M. Q. Ding Diam Relat Mater 10 (11): 1952-1961 NOV 2001

(2) E. Kohn, P. Gluche and M. Adamschik, Diam Relat Mater 8 (2-5): 934-940 MAR 1999

(3) W. F. Wei and W. J. Leivo, "Photoelectric emission and work function of semiconducting diamond", Carbon **13**, 425 (1975)

(4) F. J. Himpsel, J. A. Knapp, J. A. van Vechten, and D. E. Eastan, "Quantum photoyield of Diamond (111)- A stable negative-affinity emitter", Phys. Rev. B **20**, 624, (1979)

(5) Cui JB, Ristein J, Stammler M, Janischowsky K, Kleber G, Ley L, "Hydrogen termination and electron emission from CVD diamond surfaces: a combined secondary electron emission, photoelectron emission microscopy, photoelectron yield, and field emission study", Diamond Diam Relat Mater, 9: (3-6) 1143-1147 Apr-May 2000

(6) Sowers A. T., Ward B. L., English S. L., Nemanich R. J., "Measurement of field emission from nitrogen-doped diamond films", Diam Relat Mater, 9: (9-10) 1569-1573 Sep-Oct 2000

(7) A. T. Collins and W. S. Williams, "The nature of the acceptor center in semiconducting diamond", J. Phys. C.: Solid State Phys. 4 (1970) 1789-1800

(8) S. A. Kajihara, A. Antonelli and J. Bernholc, "Nitrogen and potential n-type dopants in diamond", Phys. Rev. Lett. **66** (1991) 2010-2013

(9) H. Zhou, Y. Yokoi, H. Tamura, S. Takami, M. Kubo, A. Miyamoto, M. N.-Gamo T. Ando, Jpn. J. Appl. Phys. 40 (2001) 2830-2832.

(10) I. Sakaguchi, M. N.-Gamo, Y. Kikuchi, E. Yasu H. Haneda, Phys. Rev. B 60 (1999) R2139-R2141

(11) M.T. Kuo, P.W. May M.N.R. Ashfold, Diam Relat Mater 11 (2002) 1422-1428

(12) S. Gupta, B.R. Weiner G. Morell, Diam Relat Mater 10 (2001) 1968-1972.

(13) Ade H., Yang W., English S. L., Hartman J., Davis R. F., Nemanich R.J., Litvinenko V. N., Pinayev I. V., Wu Y., Madey J. M. J., "A free electron laser-photoemission electron microscope system (FEL-PEEM)", Surf. Rev. Lett., 5: (6) 1257-1268 Dec 1998

(14) J. W. Vandersande, and L. D. Zoltan, "High temperature electrical conductivity measurements of natural diamond and diamond films", Surf. And Coatings Techn. **47**, 392 (1991)

(15) O. Gröning, O.M. Küttel, P. Gröning, and L. Schlapbach, J. Vac. Sci. Technol. B 17(5) Sep/Oct 1999, pp. 1970-1986

(16) L. Nilsson, O. Groening, O. Kuettel, P. Groening, and L. Schlapbach, J. Vac. Sci. Technol. B 20(1), Jan/Feb 2002

(17) A.V. Karabutov, V.D. Frolov, S.M. Pimenov, V.I. Konov, Diamond and Related Materials, 8 (1999) 763-767

(18) H. Zhou, Y. Yokoi, H. Tamura *et al.*. *Jpn. J. Appl. Phys.* **40** (2001), pp. 2830–832.

(19) I. Sakaguchi, M.N. Gamo, Y. Kikuchi, E. Yasu and H. Haneda. Phys. Rev. B 60 (1999), pp. R2139–R2141.

(20) S. Gupta, B.R. Weiner and G. Morell. Diam Relat Mater. 10 (2001), pp. 1968–1972

(21) F. Cleri, P. Keblinski, L. Colombo, D. Wolf and S.R. Phillpot. *Europhys. Lett.* **46** 5 (1999), pp. 671–677

(22) Diamond: Electronic Properties and Applications, Lawrence S. Pan and Don R. Kania editors, Kluwer Academic Publishers 1995

(23) Field, Thermionic, and Secondary Electron Emission Spectroscopy, A. Modinos, Plenum Press 1984